Int. J. Electrochem. Sci., 16 **(2021)** Article Number: 211015, doi: 10.20964/2021.10.14

International Journal of
ELECTROCHEMICAL
SCIENCE
www.electrochemsci.org

Influence of lead(II) sulphide on the formation and superconductivity of $(Tl_{1-x}Pb_x)Sr_2CaCu_2O_7$ (x = 0.1 – 0.8)

J. Nur-Akasyah, M. A. F. Nur-Diyana, R. Abd-Shukor[*]

Department of Applied Physics, Universiti Kebangsaan Malaysia, 43600 Bangi, Selangor, Malaysia
[*]E-mail: ras@ukm.edu.my

Received: 23 May 2021 / *Accepted:* 18 July 2021 / *Published:* 10 September 2021

The influence of lead(II) sulphide (PbS) on the formation and superconducting behaviour of $(Tl_{1-x}Pb_x)Sr_2CaCu_2O_7$ (Tl-1212) phase for x = 0.1, 0.3, 0.4. 0.5, 0.7 and 0.8 was investigated. The samples were prepared using the solid-state reaction method. Lead(II) sulphide was used as the source for Pb. The XRD patterns showed majority Tl-1212 phase along with other impurity phases including $PbSO_3$. The highest onset transition temperature, $T_{c\text{-onset}}$ = 104 K was observed in the x = 0.8 sample. This is higher than $(Tl_{0.4}Pb_{0.6})Sr_2CaCu_2O_7$ prepared using PbO where $T_{c\text{-onset}}$ = 97 K. The average nanoscale crystalline grain size calculated based on the Scherrer-Warren equation was in the range of 22-101 nm. AC susceptibility measurements showed that the transition temperature, $T_{c\chi}$, increased as PbS content was increased. This works showed that diamagnetic PbS enhanced the electrical properties of individual superconducting grains for Tl-1212 phase. The effectiveness of PbS versus PbO on the Tl-1212 superconductor is also discussed in this paper.

Keywords: Tl-1212 phase; lead(II) sulphide; intergranular coupling

1. INTRODUCTION

Most studies of Pb substitution on the high temperature superconductor (HTSC) family have only focused on PbO as the starting materials [for example, 1–5]. As for the thallium-based HTSC, PbO with micron-sized and nano-sized powders were used as a source for Pb. Single substitution of Pb at the Tl-site of $TlSr_2CaCu_2O_7$ (Tl-1212) phase has been studied due to the fact that Pb is next to Tl in period VI of the periodic table. Pb also possesses almost similar electronic configuration with Tl and is relatively close in terms of their chemical properties.

In single substitution studies, PbO has been used as the starting materials for $Tl_{0.5}Pb_{0.5}Sr_2CaCu_2O_7$ where the transition temperature, T_c increases up to 85 K [1,2]. Pb substitution at Tl-site of $Tl_{0.4}Pb_{0.6}Sr_2CaCu_2O_7$ showed T_c up to 97 K [3]. Nanosized PbO in $Tl_{0.4}Pb_{0.6}Sr_2CaCu_2O_7$

showed T_c at around 89 K [4]. A study of $(Tl_{0.5}Pb_{0.5-x}M_x)Sr_2CaCu_2O_7$ with M = Bi and Cr showed that Pb and Bi are effective in enhancing the T_c and stabilizing the Tl-1212 phase [5]. In $Tl_{0.5}Pb_{0.5}Sr_{1.8}Yb_{0.2}CaCu_2O_7$, superconducting transition temperature up to 105 K has been recorded [6]. While in $Tl_{0.6}Pb_{0.4}(Sr,Ba)CaCu_2O_7$ sample, a single Tl-1212 phase was achieved with T_c of 118 K when heated at 970 °C [7].

Many studies have been conducted on the substitution/addition of metal oxide, compared to metal sulphide as the starting materials of the copper oxide based HTSC. Metal sulphide is of interest since sulphur is in the same group as oxygen in the periodic table. Sulphur also has almost similar electronic configuration with oxygen.

Lead(II) sulphide (PbS) is a diamagnet with narrow band gap of 0.37 eV in the IV-VI semiconductor class and useful for optoelectronic devices [8]. In the past few years it has contributed to solar cell applications [9] and thermophotovoltaics due to its optical [10], magnetic and electrical properties [11,12]. PbS is also superconducting at around 5 [13] and 6.3 K [14].

There are few reports on the effects of PbS on the cuprate superconductors. In the $YBa_2Cu_3O_{7-\delta}$ (Y-123) superconductor PbS has been used to study the metallurgical reactions and magnetic field shielding phenomenon [15]. The study showed that Pb reacted with Ba and forming the $BaPbO_3$ phase. Partial substitution of PbS into $YBa_2Cu_{3-x}O_{7-\delta}(PbS)_{3-x}$ with $x = 0 – 0.10$ suppressed the superconducting transition temperature, T_c. The study also showed that less porous microstructure was formed which improves the magnetic field shielding properties and current density. Another report on $YBa_2Cu_{3-x}O_{7-\delta}(PbS)_{3-x}$ superconductor found that the sintering time generally decreases with the increase in PbS addition [16]. Hence, the synthesis process of $YBa_2Cu_{3-x}O_{7-\delta}$ was improved which resulted in reducing the voids.

A recent study of PbS addition on $GdBa_2Cu_3O_{7-\delta}$ (Gd-123) with $x = 0$ - 0.5 showed that PbS helped to maintain the Gd-123 phase [17]. However, PbS was found to suppress the inter-granular coupling and reduced the flux pinning energy. The use of PbS in Tl-based high temperature superconductors has not been reported extensively. PbS is of interest due to its excellent electrical properties.

It is interesting to compare the effectiveness of PbS versus PbO in stabilizing the Tl-1212 phase. PbS may form a more favourable environment between the superconducting grains where better electrical contacts may occur. Furthermore, PbS has a slightly higher melting point (1118 °C) than the sintering temperature (1000 °C) which can affect the formation of Tl-1212 phase. The objective of this work was to investigate the effects of PbS on $(Tl_{1-x}Pb_x)Sr_2CaCu_2O_7$ superconductor with $x = 0$ - 0.80. Results from X-ray diffraction (XRD), field emission scanning electron microscope (FESEM), energy dispersive X-ray analysis (EDX), electrical resistance measurements and AC susceptibility measurements are discussed in this paper.

2. EXPERIMENTAL DETAILS

Samples with nominal starting composition $(Tl_{1-x}Pb_x)Sr_2CaCu_2O_7$ with $x = 0.1$, 0.3, 0.4, 0.5, 0.7 and 0.8 were synthesized using the solid-state reaction method. Appropriate amounts of high purity

(99.9+%) powders of SrO, CaO and CuO were mixed and ground in an agate mortar. The powders were heated for 48 h at 900 °C with several intermittent grindings to obtain homogenous powder. Appropriate amounts of Tl_2O_3 and PbS were then added to the precursor and completely mixed. Due to the volatility of Tl_2O_3 at high temperature, excess 10% Tl_2O_3 was added to compensate for thallium loss during heating. The powders were then pressed into pellets with 13 mm diameter and 2 mm thickness. The pellets were then put in an alumina boat and placed in a preheated tube furnace at 1000 ºC in flowing oxygen for 4 min followed by furnace cooling to room temperature.

Powder X-ray diffraction method using Bruker model D8 Advance diffractometer with CuK_α radiation source was used to determine the phase. The lattice parameters were measured by employing the Pawley method. The Scherrer–Warren equation [18,19] with formula,

$$D = 0.941\lambda / \beta \cos \theta_\beta$$

where D is the grain size, λ is the wavelength of X-ray (1.5406 Å), β is the FWHM (full width at half maximum) of the highest intensity peak, and θ is the corresponding angle of the peak was used to calculate the nanoscale crystallite size.

Field emission scanning electron microscope (FESEM) micrographs were recorded by Merlin Gemini scanning electron microscope to determine the microstructure of the sample. The grain size was measured by using ImageJ software via the average grain size based on 100 different grains. The elemental composition of the samples was characterized by the Energy Dispersive X-Ray analysis (EDX) using an Oxford Instrument Analyzer.

The DC electrical resistance versus temperature measurements from 25 to 300 K were carried out using four-probe method with silver paste contacts in conjunction with a closed cycle refrigerator from CTI Cryogenics Model 22 and a temperature controller from Lake Shore Model 330. A constant current source between 1 and 100 mA was used throughout the measurements.

The AC susceptibility measurements from 20 to 120 K were performed by an AC susceptometer from Cryo Industry model number REF-1808-ACS. The samples were cut into bar shape for this measurement. The frequency used for the AC signal was 295 Hz and the applied magnetic field was H_{ac} = 5 Oe. The intergranular critical current density at the peak temperature of χ", $J_c(T_p)$ was calculated using the Bean model [20] with formula,

$$J_c(T_p) = H_{ac}/(lw)^{1/2}$$

where H_{ac} is the applied field, l and w are the dimensions of the cross section of the bar-shaped sample.

3. RESULTS AND DISCUSSION

The powder X-ray diffraction patterns of $(Tl_{1-x}Pb_x)Sr_2CaCu_2O_7$ are presented in Figure 1(a) for x = 0.1, 0.3 and 0.4 and Figure 1(b) for x = 0.5, 0.7 and 0.8. The x = 0.1 – 0.5 samples exhibited major Tl-1212 phase and other minor phases including $TlSr_2CuO_5$ (Tl-1201), $Ca_{0.3}Sr_{0.7}CuO_2$ (CSCO) and $Sr(SO_4)$. Tl-1212 phase showed tetragonal structure (space group P4/mmm). Tl-1201, CSCO and $Sr(SO_4)$ are orthorhombic with space group Pmmm (47), Cmcm (63) and Pbnm (62), respectively. As for x = 0.7 and 0.8 samples, $PbSO_3$ phase with monoclinic structure (space group P21/mm (11)) was also found together with the four phases. The reflection peaks from Tl-1212, Tl-1201, CSCO, $Sr(SO_4)$ and

$PbSO_3$ phases are indicated with (*hkl*), (L), (C), (S), and (Δ), respectively. Other unmarked peaks observed in $x \geq 0.3$ samples may be caused by unreacted starting materials.

Figure 1(a)

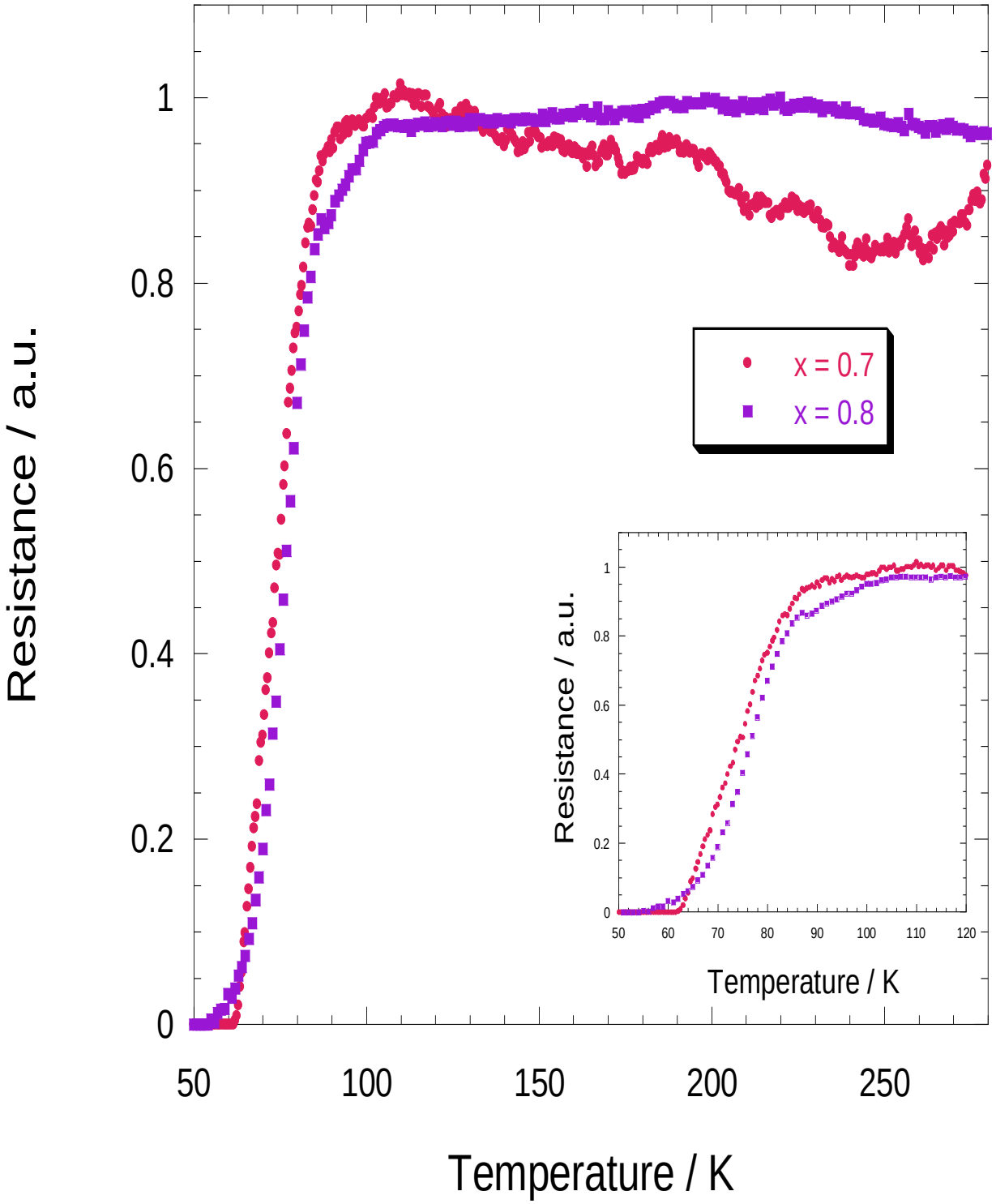

(a)

Figure 1(b)

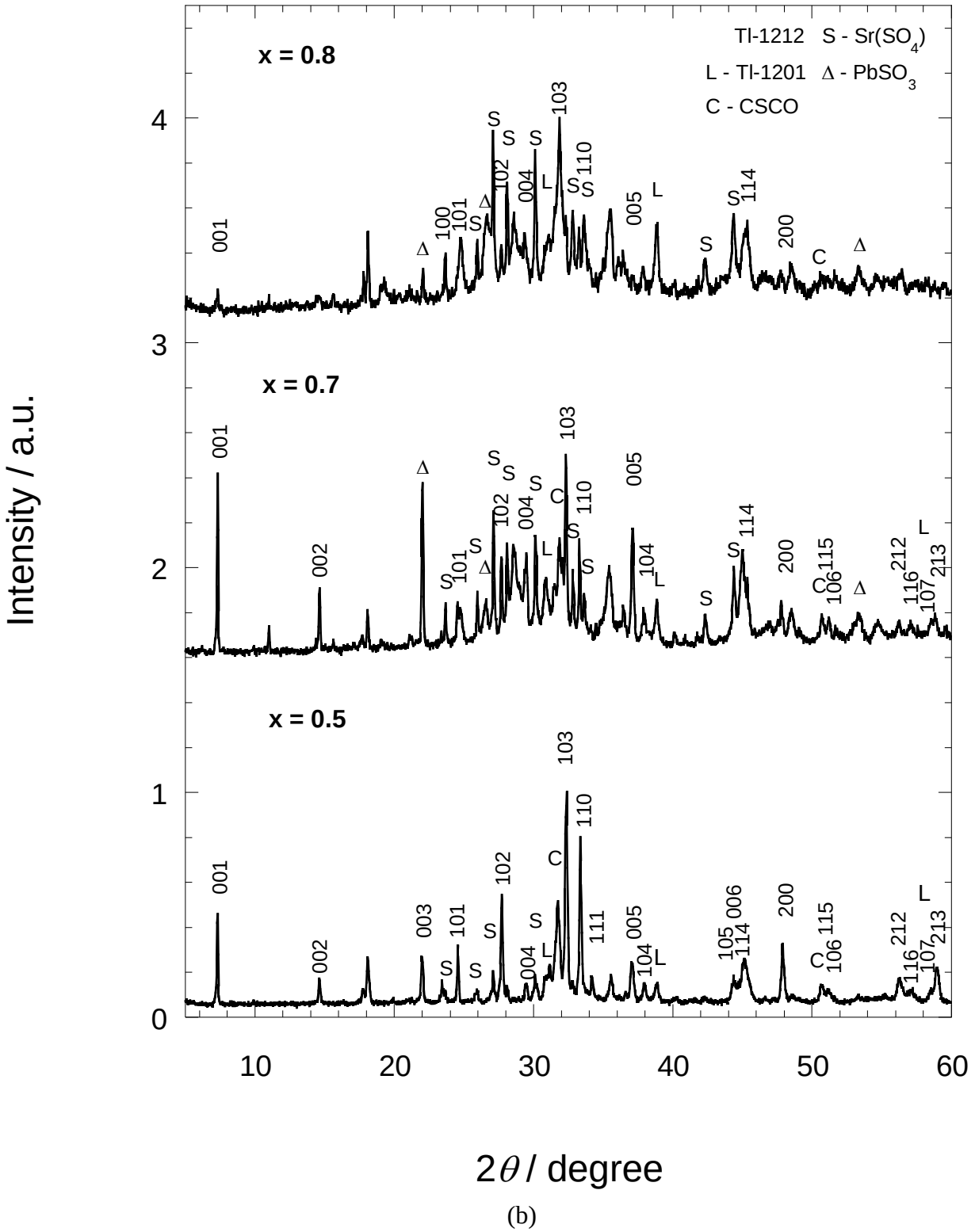

(b)

Figure 1. XRD patterns of $(Tl_{1-x}Pb_x)Sr_2CaCu_2O_7$ for (a) x = 0.1 - 0.4 and (b) x = 0.5 - 0.8. Peaks with Tl-1201, CSCO, $Sr(SO_4)$ and $PbSO_3$ phases are indicated with (L), (C), (S) and (Δ), respectively

XRD patterns (Figure 1) shows that PbS with higher melting point (1118 °C) than the sintering temperature (1000 °C) stabilized the Tl-1212 phase, but other phases were also observed. This result is in agreement with the study of PbS-doped Y-123 phase where further addition of PbS formed four other different phases. The phases were identified to be Y-123, Y-211, $BaPbO_3$ and CuO, respectively [15,16]. In this work, higher amounts of PbS (x = 0.7 and 0.8) resulted in the formation of $PbSO_3$ phase and decreased in the Tl-1212 phase. A previous study showed that PbS addition maintained the Gd-123 phase in the $GdBa_2Cu_3O_{7-\delta}(PbS)_x$ samples with x = 0, 0.2, 0.3, 0.4 and 0.5 [17].

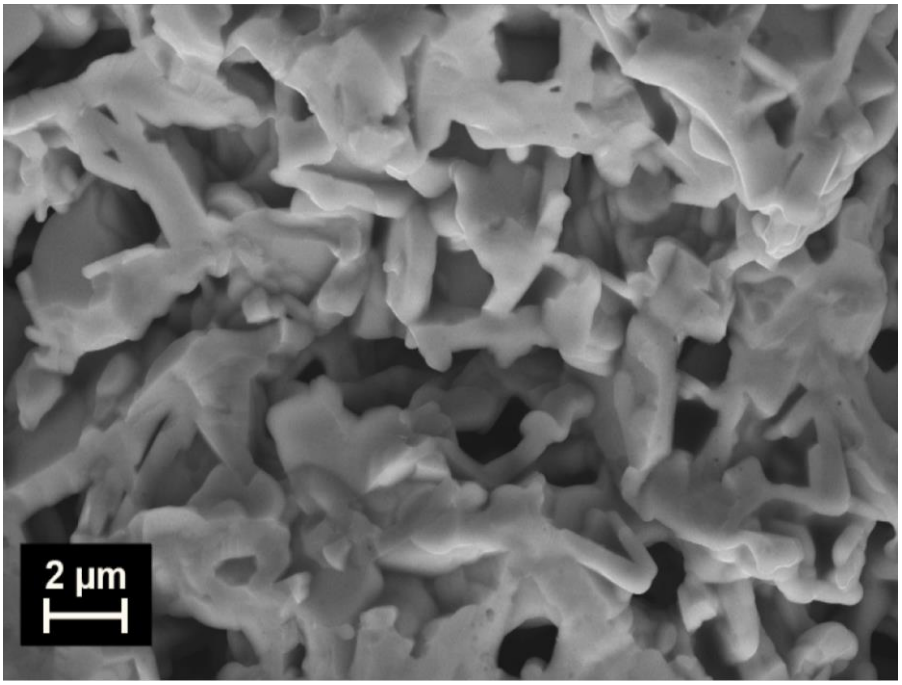

(a)

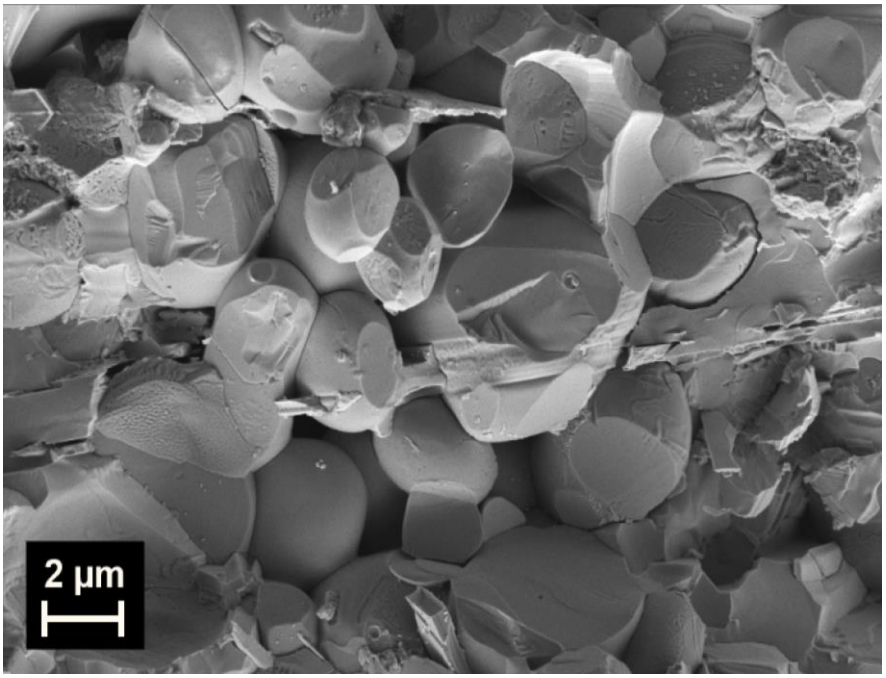

(b)

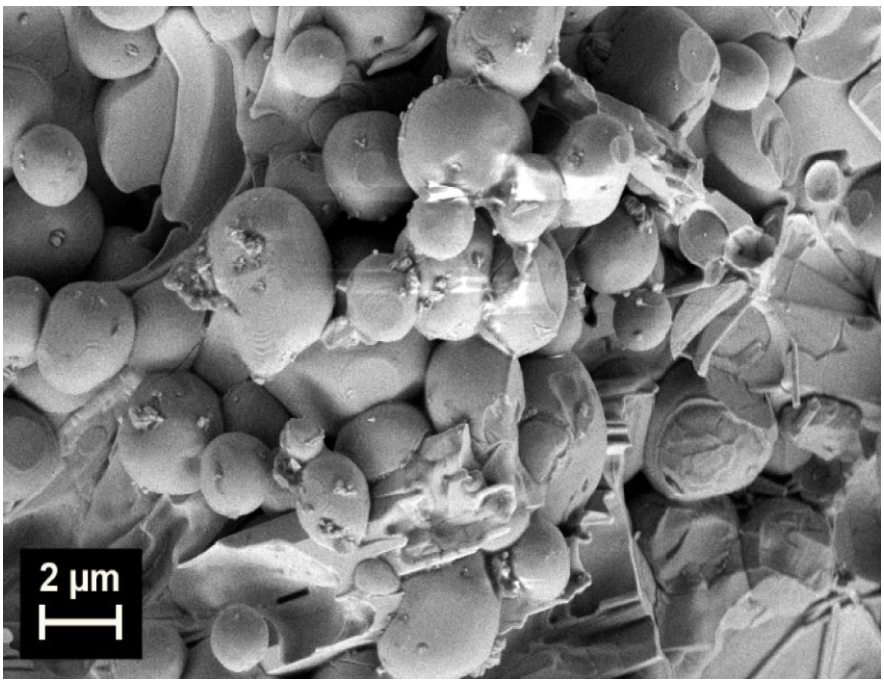

(c)

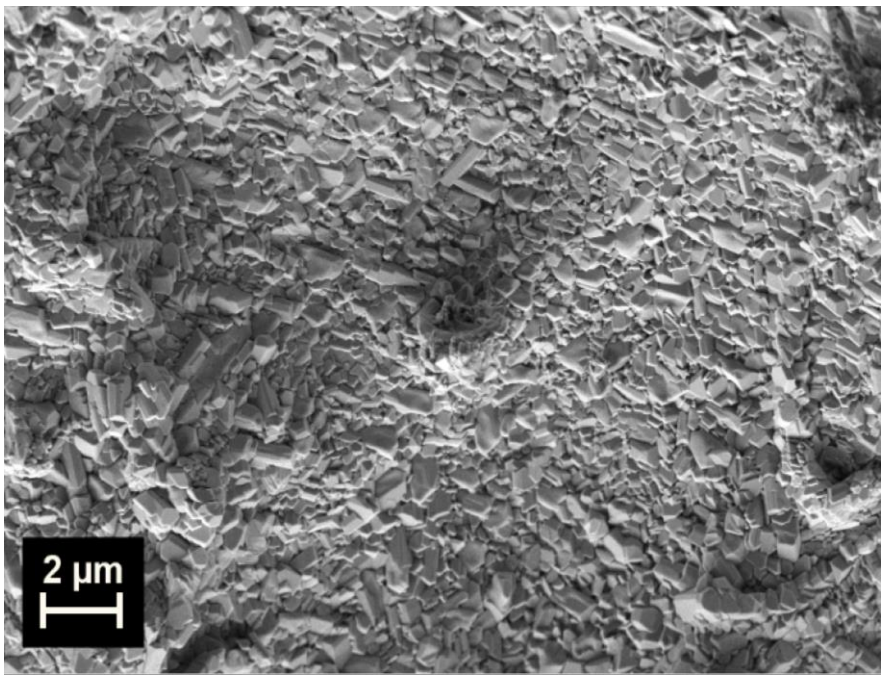

(d)

Figure 2. FESEM micrographs of $(Tl_{1-x}Pb_x)Sr_2CaCu_2O_7$ for (a) $x = 0.1$, (b) $x = 0.4$, (c) $x = 0.5$ and (d) $x = 0.8$

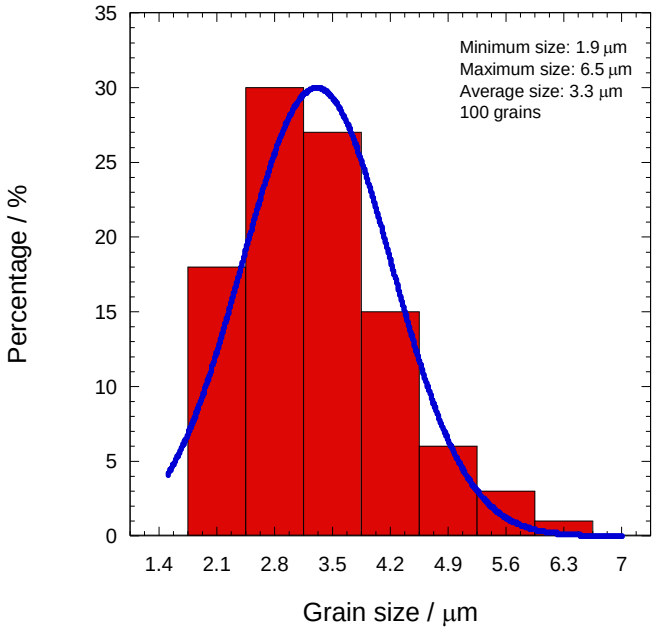
Minimum size: 1.9 μm
Maximum size: 6.5 μm
Average size: 3.3 μm
100 grains
Percentage / %
Grain size / μm
0
5
10
15
20
25
30
35
1.4
2.1
2.8
3.5
4.2
4.9
5.6
6.3
7

(a)

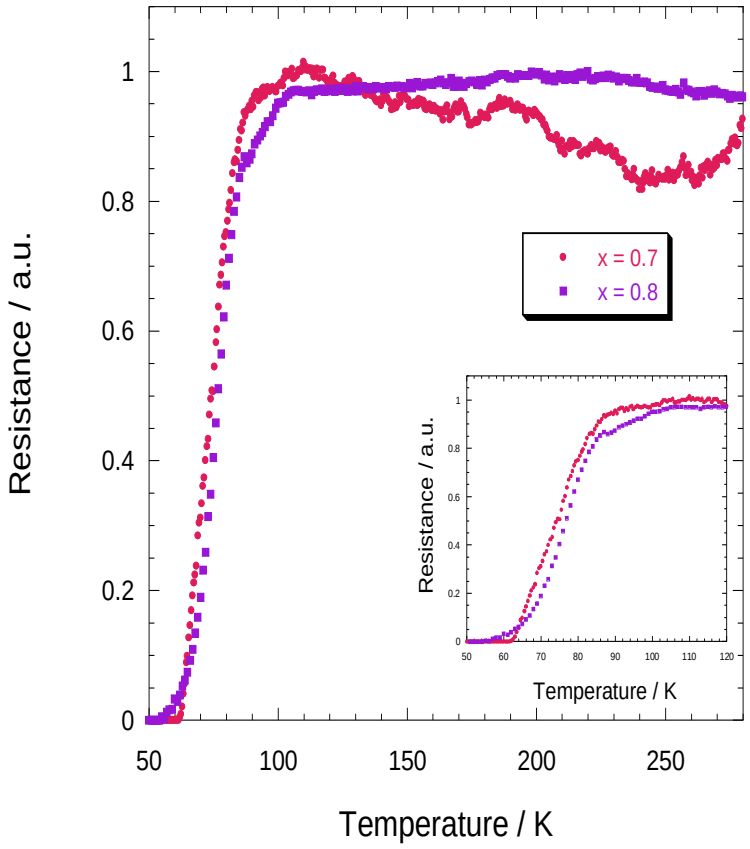
x = 0.7
x = 0.8
Resistance / a.u.
Temperature / K
0
0.2
0.4
0.6
0.8
1
50
100
150
200
250

(b)

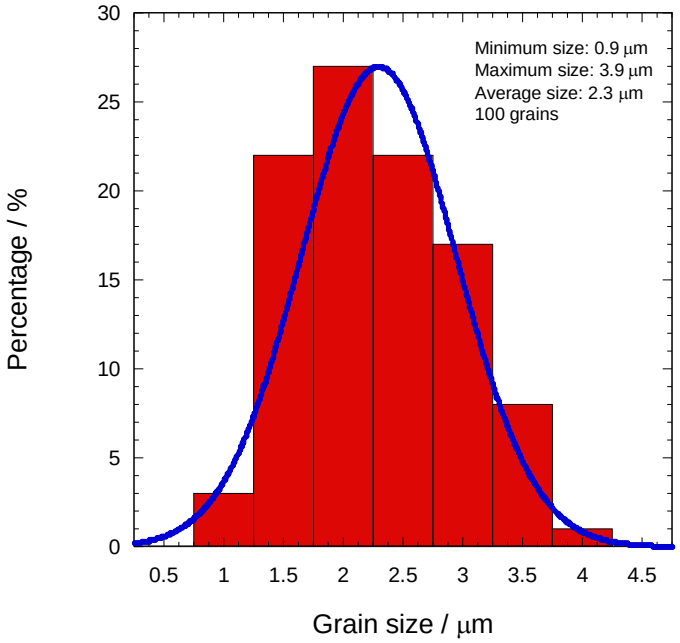

(c)

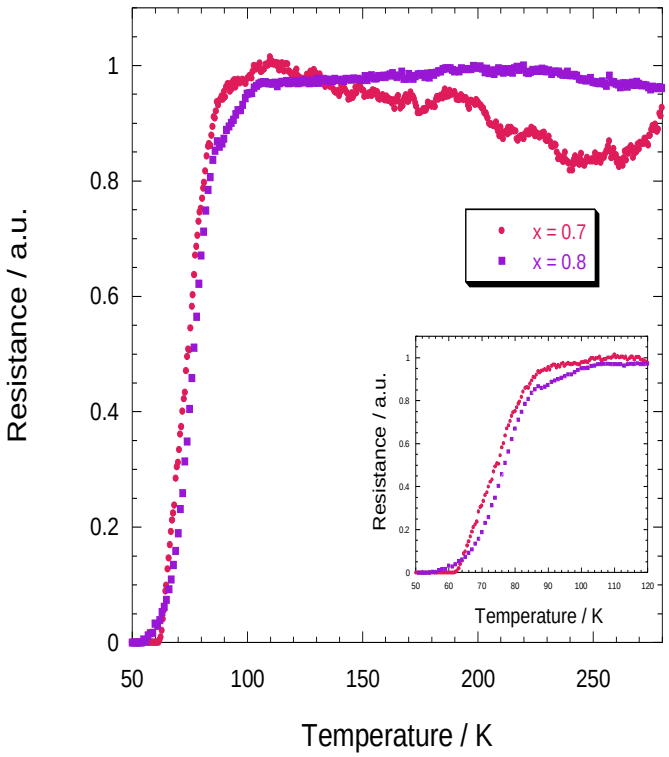

(d)

Figure 3. Grain size of $(Tl_{1-x}Pb_x)Sr_2CaCu_2O_7$ for (a) $x = 0.1$, (b) $x = 0.4$, (c) $x = 0.5$ and (d) $x = 0.8$

The nanoscale crystalline grain size measured using on the Scherrer-Warren equation, was found to increase as the PbS content was increased, i.e. up to 101 nm (x = 0.7) and then decreased to 26 nm for 0.8 sample (Table 1).

Table 1. $T_{c\text{-onset}}$, $T_{c\text{-zero}}$, ΔT_c, $T_{c\chi'}$, T_p, J_c (T_p) and nanoscale crystalline grain sizes of $(Tl_{1-x}Pb_x)Sr_2CaCu_2O_7$ (x = 0.1 - 0.8)

x	$T_{c\text{-onset}}$ / K	$T_{c\text{-zero}}$ / K	ΔT_c / K	$T_{c\chi'}$ / K	T_p / K	$J_c(T_p)$ / A cm^{-2}	Crystallite size / nm
0.1	34	27	7	25	-	20	22
0.3	93	52	41	48	39	16	48
0.4	76	40	36	59	43	16	49
0.5	89	49	40	66	50	16	48
0.7	102	61	41	70	-	18	101
0.8	104	54	50	81	-	17	26

Figure 2 shows FESEM micrographs of $(Tl_{1-x}Pb_x)Sr_2CaCu_2O_7$ samples with x = (a) 0.1, (b) 0.4, (c) 0.5 and (d) 0.8. The microstructure of the samples showed plate-like, granular-like and close-packed rod-like structure. The histograms based on 100 grains were plotted to determine the grain size of the samples (Figure 3). The average grain size was 3.3, 3.4, 2.3 and 0.6 μm for x = 0.1, 0.4, 0.5 and 0.8 samples, respectively (Figure 3). The grain size is consistent with the crystalline grain size calculated by the Scherrer-Warren equation. PbS changed the microstructure of the sample (Figure 2). In $GdBa_2Cu_3O_{7-\delta}(PbS)_x$ samples, the microstructure was also found to change from plate-like to oblique-like structure [17]. Higher amounts of PbS (x = 0.8) showed less porosity and voids. This provided better electrical contact between the grains which is necessary to obtain higher superconducting transitions. In $YBa_2Cu_{3-x}O_{7-\delta}(PbS)_{3-x}$ and $GdBa_2Cu_3O_{7-\delta}(PbS)_x$ superconductors, lower porosity and a close-packed structure due to PbS was also observed [15–17].

The EDX spectra for $(Tl_{1-x}Pb_x)Sr_2CaCu_2O_7$ for x = 0.1, 0.4, 0.5 and 0.8 samples along with approximate elemental atomic and weight percent are presented in Figure 4(a), 4(b), 4(c) and 4(d), respectively. The peaks of Tl, Sr, Ca, Cu and O were observed in all samples. EDX spectra in Figure 4 also confirmed the presence of Pb and S.

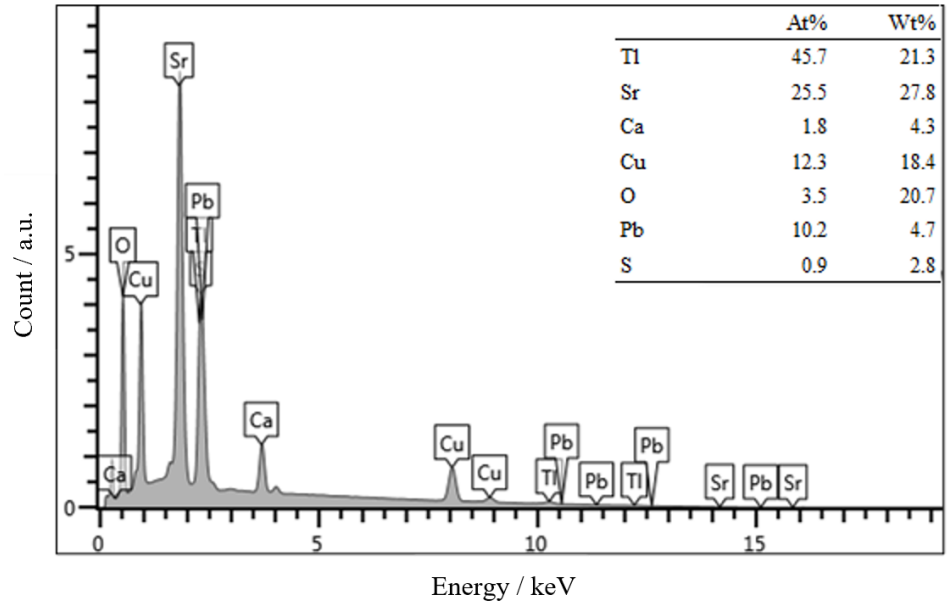

	At%	Wt%
Tl	45.7	21.3
Sr	25.5	27.8
Ca	1.8	4.3
Cu	12.3	18.4
O	3.5	20.7
Pb	10.2	4.7
S	0.9	2.8

(a)

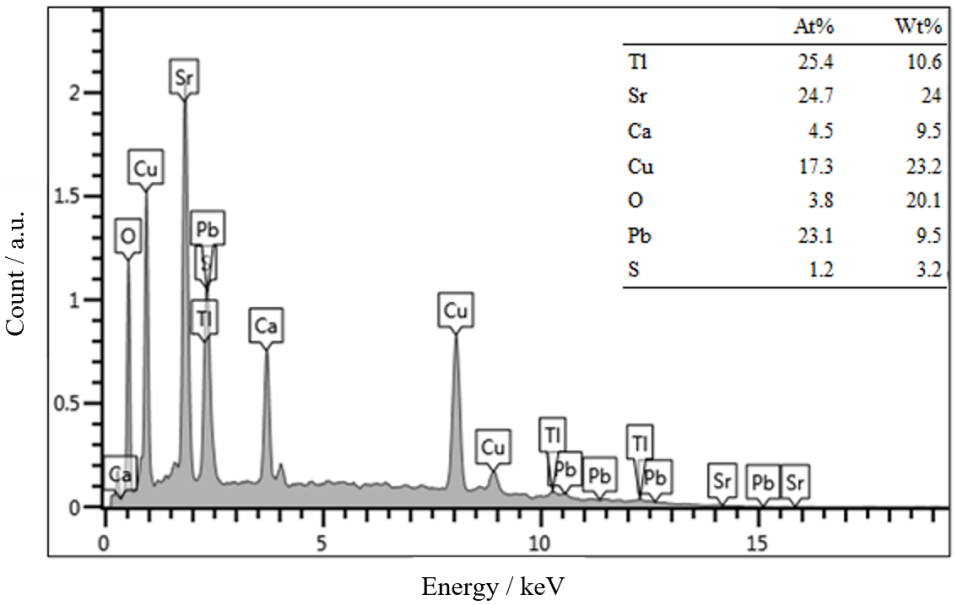

	At%	Wt%
Tl	25.4	10.6
Sr	24.7	24
Ca	4.5	9.5
Cu	17.3	23.2
O	3.8	20.1
Pb	23.1	9.5
S	1.2	3.2

(b)

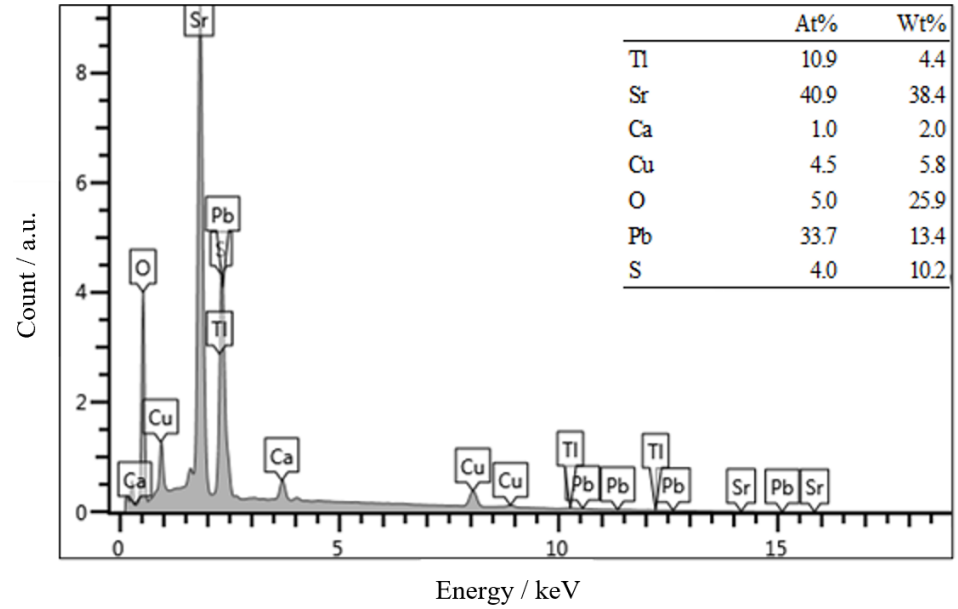

(c)

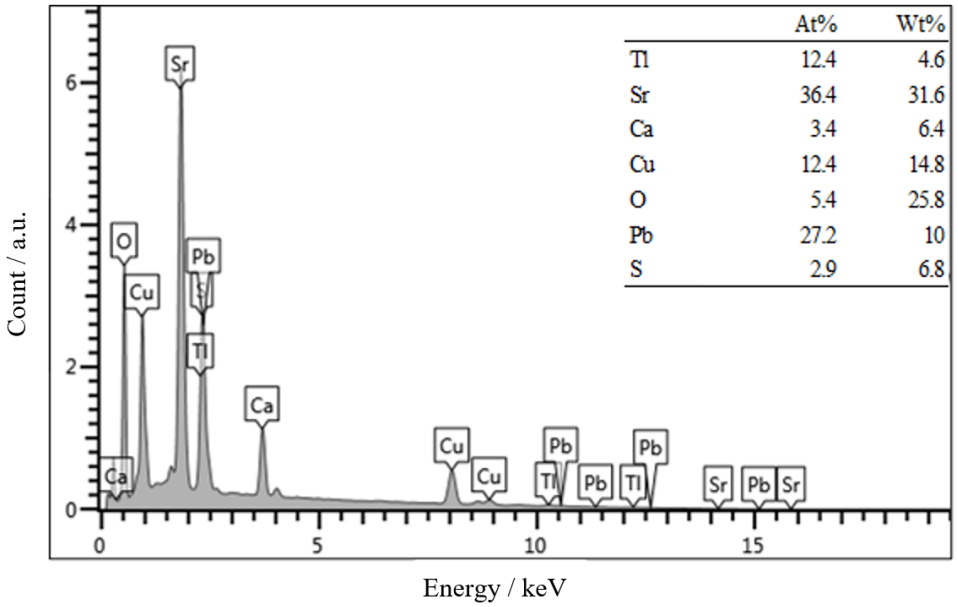

(d)

Figure 4. EDX spectra of $(Tl_{1-x}Pb_x)Sr_2CaCu_2O_7$ for (a) $x = 0.1$, (b) $x = 0.4$, (c) $x = 0.5$ and (d) $x = 0.8$. Insert shows the atomic and weight percentage of the related elements

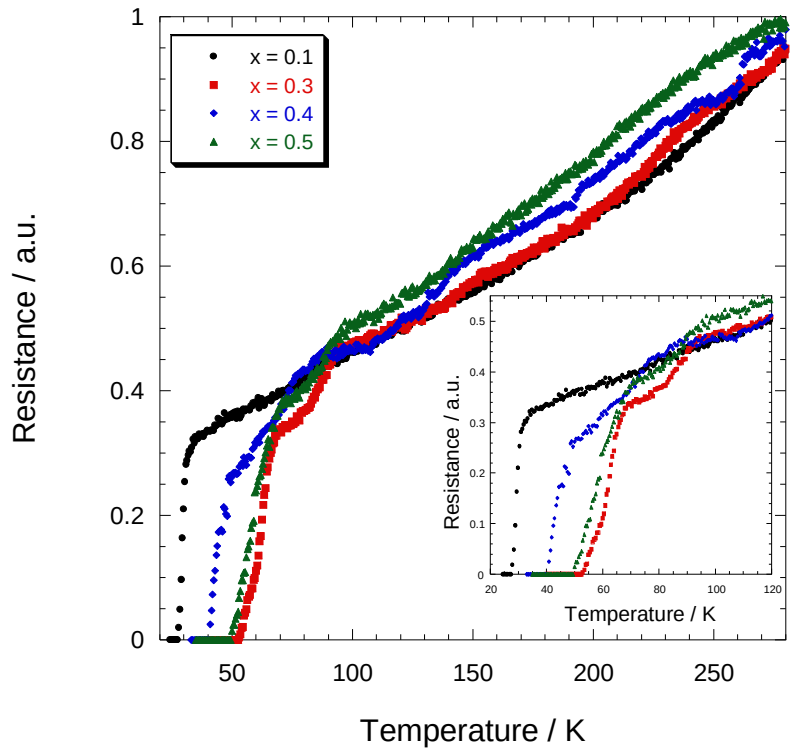

(a)

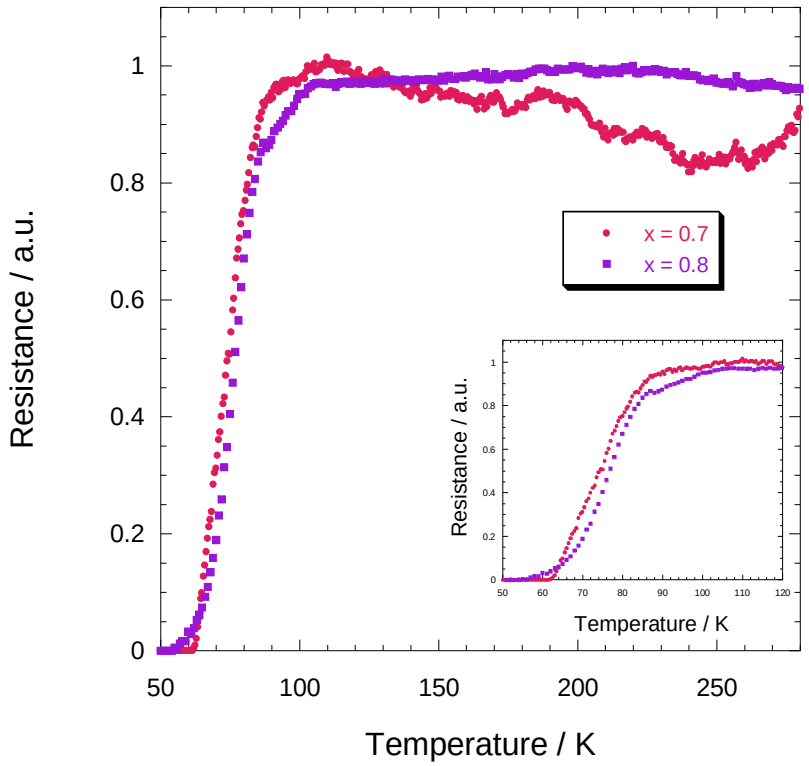

(b)

Figure 5. Electrical resistance versus temperature of $(Tl_{1-x}Pb_x)Sr_2CaCu_2O_7$ for (a) x = 0.1 - 0.5 and (b) x = 0.7 - 0.8. Insets show the electrical resistance of the samples for temperature between (a) 20 K - 120, and (b) 50 K - 120 K.

The normalized electrical resistance versus temperature curves of all samples is shown in Figure 5(a) and 5(b). A metallic normal state behaviour above the onset temperature, $T_{c\text{-onset}}$ was observed in all samples except for x = 0.7 and 0.8 which showed a semiconductor like behaviour. There was a significant variation in $T_{c\text{-onset}}$ (34–104 K) and zero-resistance temperature, $T_{c\text{-zero}}$ (27-61 K). $T_{c\text{-onset}}$ was highest for x = 0.8 (104 K). This is much higher than $(Tl_{0.4}Pb_{0.6})Sr_2CaCu_2O_7$ with $T_{c\text{-onset}}$ = 97 K where PbO was used as the source of Pb [3]. These results indicated that PbS enhanced the transition temperature of individual superconducting grains. Although the x = 0.8 sample showed the highest $T_{c\text{-onset}}$, the normal state was not optimized as shown by the semiconducting behaviour. This sample also showed another transition at 90 K.

Double superconducting transition was observed in the x = 0.3, 0.4, 0.5 and 0.8 samples (Figure 5). This was due to the presence of another superconducting phase Tl-1201 and other impurity phases such as CSCO, $Sr(SO_4)$ and $PbSO_3$ that weakened the coupling strength among grains. In this work, superconducting transition temperature up to 104 K (x = 0.8) has been observed by using PbS in the Tl-1212 superconductor. However, the use of PbO enhances the formation of the Tl-1212 phase [1-4]. This indicated that PbO provided better environment between the structural blocks of the thallium cuprates where lattice mismatch may occur. However, the highest transition temperature for samples prepared using PbO was only 97 K. Our result indicated that PbS did not enhance the formation of Tl-1212 phase, but it enhanced the transition temperature to 104 K for the x = 0.8 samples.

$T_{c\text{-zero}}$ is dependent on the Tl-1212 phase, homogeneities and the intergranular characteristics [21,22]. PbS did not enhanced the formation of the Tl-1212 phase. Further amounts of PbS resulted in weak links and worsened the connectivity between the grain boundaries [23,24]. By comparison, Bi substitution in Tl-1212 showed some improvements in the superconducting phase formation [25].

The AC susceptibility versus temperature for all samples are shown in Figures 6(a) and 6(b). The AC susceptibility onset transition temperature of bulk superconductivity, $T_c\chi'$ is indicated by the sudden decrease in the real part, χ' of the complex susceptibility ($\chi = \chi' + i\,\chi''$). The curves show the transition from the paramagnetic state to diamagnetic shielding of the samples. Two peaks should be observed in the imaginary part of the susceptibility χ'' which indicates AC losses. A narrower peak at high temperature indicates the intrinsic losses (intragrain coupling) while a broad peak at low temperature represents the intergrain coupling losses. There are no intrinsic peaks in Figures 6(a) and 6(b) due to the relatively low applied fields used in this measurement.

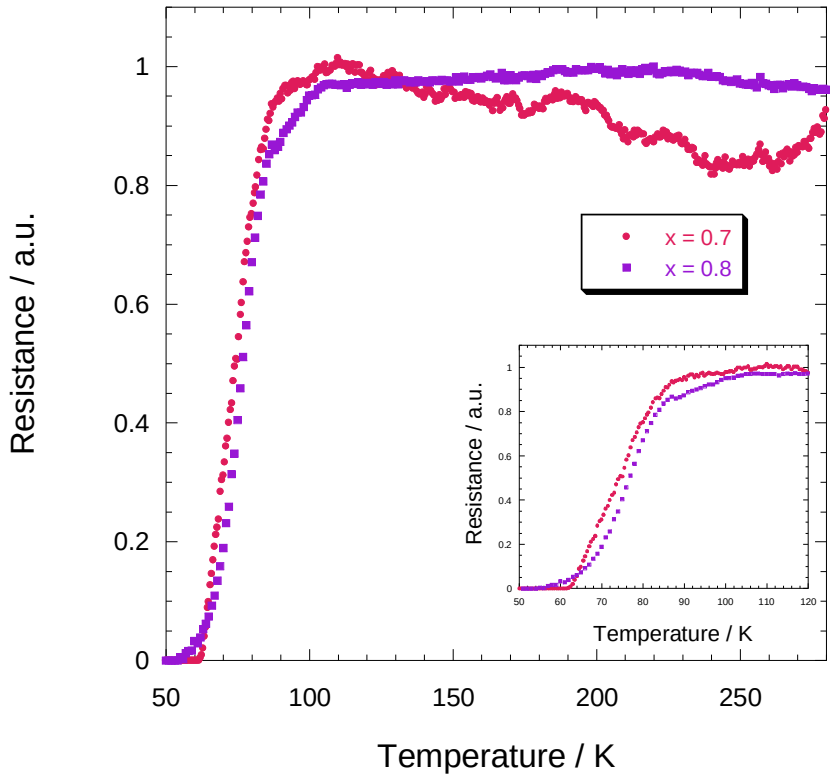

(a)

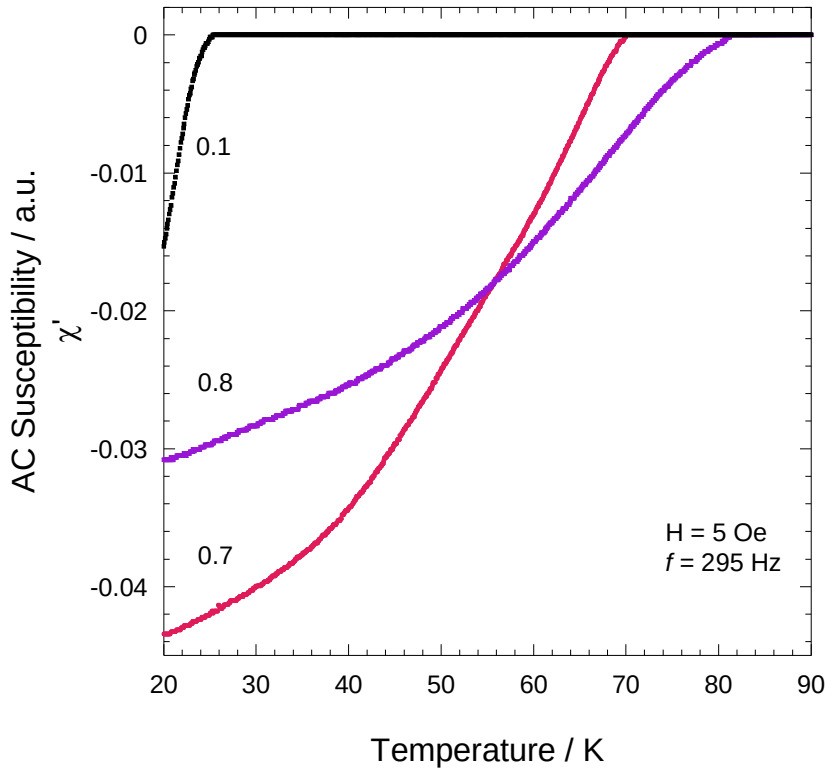

(b)

Figure 6. AC susceptibility versus temperature of $(Tl_{1-x}Pb_x)Sr_2CaCu_2O_7$ for (a) x = 0.3 - 0.5 and (b) x = 0.1, 0.7 - 0.8

The highest $T_{c\chi'}$ was observed in the $x = 0.8$ sample which was 81 K. In general, $T_{c\chi'}$ increased with increase in PbS content (Figure 6). The peak temperature (T_p) of the imaginary part of the susceptibility, χ" shifted to higher temperature and was narrower for $x = 0.3$ to 0.5 (Figure 6(a)). However, T_p was not observed in $x = 0.1$, 0.7 and 0.8 samples within the measured temperature range, 20 to 120 K (Figure 6b). The T_p of the samples might be below 20 K which signified a weak intergranular coupling and suppressed flux pinning force in certain samples. These results are in a good agreement with the FESEM micrographs that showed a smaller grain size in $x = 0.1$ and 0.8 samples as shown in Figure 2(a) and 2(d), respectively. Previous study also indicated that PbS addition weakened the intergranular coupling of $GdBa_2Cu_3O_{7-\delta}$ superconductor [17].

In general, the magnitude of the applied magnetic field, H_{ac} is equal to the penetrated flux at T_p. Thus, the intergranular critical current density, J_c at T_p can be measured by using Bean model [20]. The $J_c(T_p)$ for $(Tl_{1-x}Pb_x)Sr_2CaCu_2O_7$ samples lies within 16 - 20 A cm^{-2}. The $T_{c\text{-onset}}$, $T_{c\text{-zero}}$, ΔT_c, $T_{c\chi'}$, T_p, $J_c(T_p)$ and nanoscale crystalline grain sizes of $(Tl_{1-x}Pb_x)Sr_2CaCu_2O_7$ are shown in Table 1. Our results showed that PbS suppressed the magnetic properties more than the electrical properties based on the comparison between $T_{c\text{-onset}}$, $T_{c\text{-zero}}$ with T_p. Further increase of PbS ($x = 0.7$ and 0.8) weakened intergranular coupling and lowered the flux pinning energy.

In conclusion, the effect of PbS on the formation of $(Tl_{1-x}Pb_x)Sr_2CaCu_2O_7$ (x = 0 - 0.8) superconductor have been studied. In general, $T_{c\text{-onset}}$, $T_{c\text{-zero}}$ and $T_{c\chi'}$ increased with PbS content. The highest $T_{c\text{-onset}}$ as observed in this work using PbS was 104 K, while in previous works where PbO was used, the highest $T_{c\text{-onset}}$ was 97 K. This work showed that PbS resulted in higher $T_{c\ onset}$ compared to PbO. PbS provided better environment between the superconducting grains hence, enhancing the electrical properties. However, PbS suppressed the magnetic properties by weakening the intergranular coupling and flux pinning energy although the microstructure was improved. Effects of other metal sulphide such as CdS, ZnS and FeS on the Tl-1212 phase are interesting materials for further studies.

ACKNOWLEDGMENTS
This research was supported by the Ministry of Higher Education of Malaysia under Grant No. FRGS/1/2020/STG07/UKM/01/1 and UKM under grant number MUTIARA-A163185.

References

1. C. Martin, J. Provost, D. Bourgalt, B. Domenges, C. Michel and M. Hervieu, *Phys. C*, 157 (1989) 460.
2. M. A. Subramanian, C. C. Torardi, J. Gopalakrishnan, P. L. Gai, J. C. Calabrese, T. R. Askew, R. B. Flippen and A. W. Sleight, *Science*, 242 (1988) 249.
3. R. Abd-Shukor and K. S. Tee, *J. Mater. Sci. Lett.,* 17 (1998) 103.
4. H. S. Elmasroub and R. Abd-Shukor, *AIP Conf. Proc*., 1838 (2017) 1.
5. M. Fatmasari and R. Abd-Shukor, *J. Supercond. Nov. Magn.,* 25 (2012) 747.
6. A. K. Yahya, W. F. Abdullah, H. Imad and M. H. Jumali, *Phys. C,* 463–465 (2007) 474.
7. M. G. Ranjbar, M. Ghoranneviss and R. Abd-Shukor, *Appl. Phys. A: Mater. Sci. Process,* 124 (2018) 456.

8. H. D. Jahromi and M. Moaddeli, *Mater. Res. Express,* 6 (2019) 116220.
9. S. Chatterjee and U. Pal, *Opt. Eng.,* 32 (1993) 2923.
10. T. K. Chaudhuri, *Int. J. Energy Res.,* 16 (1992) 481.
11. S. Ravishankar, A. R. Balu, K. Usharani, S. Balamurugan, D. Prabha and V. S. Nagarethinam, *Optik (Stuttg)*, 134 (2017) 121.
12. R. S. Parra, P. J. George, G. G. Sánchez, A. E. Jiménez González, L. Baños and P. K. Nair, *J. Phys. Chem. Solids*, 61 (2000) 659.
13. J. Darby, J. Hatton and B. V Rollin, *Proc. Phys. Soc. Sect. A,* 63 (1950) 1181.
14. Y. Timofeev, B. Vinogradov and E. Yakovlev, *Sov. Phys. - Solid State,* 23 (1981) 1474.
15. A. K. Tyagi and T. P. Sharma, *Mater. Lett.,* 18 (1994) 341.
16. A Tyagi, T Sharma and K Shahi, *J. Therm. Anal. Calorim.,* 44 (1995) 755.
17. M. A. Salma and R. Abd-Shukor, *Appl. Phys. A: Mater. Sci. Process.,* 126 (2020) 3.
18. O. Ozturk, E. Asikuzun and G. Yildirim, *J. Mater. Sci.: Mater. Electron.,* 24 (2013) 1274.
19. O. Ozturk, M. Erdem, E. Asikuzun, O. Yildiz, G. Yildirim, A. Varilci and C. Terzioglu, *J. Mater. Sci.: Mater. Electron.,* 24 (2013) 230.
20. C. P. Bean, *Rev. Mod. Phys*., 36 (1964) 31.
21. Y. Slimani, M. A. Almessiere, E. Hannachi, A. Baykal, A. Manikandan, M. Mumtaz and F. Ben Azzouz, *Ceram. Int.,* 45 (2019) 2621.
22. Y. Slimani, M. A. Almessiere, E. Hannachi, M. Mumtaz, A. Manikandan, A. Baykal and F. Ben Azzouz, *Ceram. Int.,* 45 (2019) 6828.
23. Y. Slimani, E. Hannachi, M. Zouaoui, F. Ben Azzouz and M. Ben Salem, *J. Supercond. Nov. Magn.,* 31 (2018) 2339.
24. M. A. Almessiere, Y. Slimani, E. Hannachi, R. Algarni and F. Ben Azzouz, *J. Mater. Sci.: Mater. Electron.,* 30 (2019) 17572.
25. A. K. Yahya, W.F. Abdullah, M.H. Jumali and R. Abd-Shukor, *Ceram. Int.*, 30 (2004) 1591